Chen, X., et al., 2020, Zinc isotope evidence for paleoenvironmental changes during Cretaceous Oceanic Anoxic Event 2: Geology, v. 49, https://doi.org/10.1130/G48198.1

GSA Data Repository

Supplemental Materials for *Zinc isotope evidence for paleoenvironmental changes during Cretaceous Oceanic Anoxic Event 2*

Authors: Xi Chen, Bradley B. Sageman, Hanwei Yao, Sheng'Ao Liu, Kaibo Han, Yi Zou, and Chengshan Wang

This file includes:

1. STUDIED SECTION

The Gongzha section is located in the Tingri area of Tibet, which tectonically belongs to the Tethys Himalayas (Fig. DR1). Late Cenomanian to Maastrichtian marine strata of pelagic depositional environments are well developed in this section (Wang et al., 2004). During the Cretaceous, the section was located on the northern margin of the Indian continent and the south margin of the Eastern Tethys Ocean. Because a large fraction of sediments deposited in the East Tethys Ocean were subducted beneath the Asian continent, sedimentary records in

the Tethys Himalayas provide unique opportunities to study the paleoceanography and paleoenvironment of the Cretaceous of the East Tethys realm.

The Gongzha section yields abundant and poorly to moderately preserved foraminifera, on which biostratigraphy was established (Wan et al., 2003; Li et al., 2006). Li et al. (2006) published a secular $\delta^{13}C_{carb}$ curve for Upper Cretaceous of this section. Based on bio- and chemostratigraphic correlation, the OAE 2 equivalent level is identified with the distinct $\delta^{13}C$ positive excursion at the Cenomanian-Turonian transition. The OAE 2 interval, as defined by its characteristic carbon isotope excursion (CIE) in Gongzha is ~ 28 m in thickness. The depositional environment is outer ramp (Wang et al., 2004). During field logging, Li and his colleagues painted depth numbers on the rocks every 5 meters. These marked depths acted as a coherent stratigraphic framework for subsequent studies, e.g., Li et al. (2017), Zhang et al. (2019), and this study.

Although anoxic to euxinic conditions prevailed during OAE 2 in many basins, evidence does not suggest the same redox conditions characterized the south margin of the eastern Tethys Ocean. Elemental geochemistry, including redox indicators such as V and Cr, indicate that the water column was oxygenated during the event (Bomou et al., 2013). In contrast to these observations, recent $\delta^{15}N$ data were interpreted to reflect expansion of an anoxic environment during the C-T interval (Zhang et al., 2019), however, the $\delta^{15}N$ record from Gongzha does not show the significant negative excursions observed in other OAE2 sites and interpreted to reflect nutrient and redox dynamics (Kuypers et al., 2004; Junium and Arthur, 2007).

Age constraints for OAE 2 in this section are based on planktonic foraminifera and an

astronomical time scale (ATS). The lower 70 m of the section contains *R. cushmani*, *W. archaeocretacea*, and *H. helvetica* biozones (Wan et al., 2003; Li et al., 2006; Bomou et al., 2013). The astronomical time scale from the lower part of the Gongzha section was developed by Li et al. (2017). Based on the ATS, Li et al. (2017) estimated that the duration of the $\delta^{13}C$ excursion (defined by return to background $\delta^{13}C$ values) is ~870 kyr (this is the longer of two common definitions of the event discussed in the literature: e.g., Sageman et al., 2006). They divided the $\delta^{13}C$ curve across OAE 2 into 6 segments, including pre- and post-excursion units.

This study largely followed the scheme of Li et al. (2017) to divide the segments of $\delta^{13}C$ curve across OAE 2, except for interpretation of the initial onset of the OAE 2 carbon isotope excursion. There is a fairly consistent background $\delta^{13}C_{carb}$ signal with relatively minor variance in strata prior to the OAE 2 positive excursion (from the base to ~40 m), defined as segments C1 and C2. Although initiation of the OAE 2 CIE was placed at ~37 m by Li et al. (2017), $\delta^{13}C$ values are similar to background values (< 2‰) and start to increase rapidly from ~40 m, which is recorded in the $\delta^{13}C$ dataset of both previous publications (Li et al., 2017) and this study (Fig. 2). Therefore, we suggest that the OAE 2 CIE initiates at ~40 m in the section. Segment C3 (from ~40 m to ~48 m) is characterized by rapid increase in values of $\delta^{13}C_{carb}$, marking the onset of OAE 2 and lasting for ~280 kyrs. In segment C4 (from ~48 m to 64 m; ~350 kyr), the $\delta^{13}C_{carb}$ values persist at ~3‰ followed by stepwise recovery of $\delta^{13}C_{carb}$ values to pre-excursion levels (segment C5). The ATS (Li et al., 2017) provides a foundation for future study on the evolution of paleoenvironment during OAE 2.

2. ANALYTICAL METHODS

2.1 Procedure for Zn isotope measurement

A leaching procedure used to prepare for Zn isotope measurements strictly followed the method of Liu et al. (2017). Samples were carefully checked to avoid visible veins and fractures, and were ground to ~ 200 mesh with an agate mortar that was carefully cleaned with Milli-Q water (18.2 MΩ). The leaching steps were performed in a clean room under laminar flow hood (class 100) to minimize Zn contamination. Hydrosoluble salts and exchangeable fraction on clays were removed before leaching of carbonates using Milli-Q water and 1 N ammonium acetate (NH_4AC), alternately. The carbonate fraction was selectively dissolved with two steps of 0.05 M super-pure acetic acid in a thermostat at 65 ℃, until no bubbles were generated. The supernatants were collected after 20 min of centrifugation, followed by filtration. The leached supernatants were dried at 80 ℃ and added with 2 ml of 8 M HCl. This step was repeated twice to remove acetic acid. Finally, the solution was prepared in 1 ml of 8 M HCl for chemical anion-exchange separation.

The leaching solutions were dried at 80 ℃. Zinc was purified by an ion-exchange chromatography using Bio-Rad strong anion resin AG-MP-1M. 2 ml pre-cleaned resin was loaded onto the column. Matrix elements were eluted in the first 10 ml of 8 N HCl. Copper and iron were then collected in the following 24 ml of 8 N HCl +0.001% H_2O_2 and 18 ml of 2N HCl. Zinc was collected in the subsequent 15 ml of 0.5N HNO_3. This procedure allows Ca to be completely separated from Zn and a 100% recovery for Zn. The Zn fractions were repeatedly dried and dissolved with 3% HNO_3 to remove all chlorine prior to isotope analysis.

Zinc isotopic ratios were measured using a Neptune plus multi-collector inductively coupled plasma mass-spectrometry (MC-ICP-MS) at the Isotope Geochemistry Laboratory of

the China University of Geosciences (Beijing). Sample-standard bracketing method was used to correct for instrumental mass fractionation. The samples and standards are run in ~200 ppb diluted solution dissolved in 3% (v) HNO_3. The take-up time is 80 s. The Zn isotope data for leaching solutions and residues are reported in Table DR. 2. Zn isotope data of the leachates are the mean of the two steps of leaching on the samples, which agree with each other within ±0.1‰. All samples analyzed in this study yield a slope of 2.08 in a $\delta^{68}Zn$–$\delta^{66}Zn$ cross-plot, which is consistent with the mass-dependent line with a slope of 2, indicating mass-dependent Zn isotope fractionation and no analytical artifacts from unresolved isobaric interferences on Zn isotopes.

2.2 Measurements of major and trace element concentrations of bulk sample

Analyses of major element concentrations were conducted at the State Key Laboratory of Geological Processes and Mineral Resources, China University of Geosciences, Beijing and the Wuhan SampleSolution Analytical Technology Co., Ltd., Wuhan, China. For elemental oxide concentration analysis, a 0.7g sample (200 mesh) was mixed with 7.0g of lithium borate and fused to glass beads. The addition of a small amount (100 mg) of the halide LiBr acted as a release agent when using platinum molds. The mixture was heated in a high frequency fusion machine at ~1000 °C, until thoroughly melted. Then the fused beads were loaded into the XRF instrument for testing on a Shimadzu wavelength dispersive X-ray fluorescence spectrometer. Concentrations of the major elements are listed in Table DR. 1.

Trace element analysis of whole rock samples were conducted on an Agilent 7700e ICP-MS at the Wuhan SampleSolution Analytical Technology Co., Ltd., Wuhan, China. The

detailed sample-digesting procedure was as follows: (1) Sample powders (200 mesh) were placed in an oven at 105□ for drying of 12 hours; (2) 50 mg sample powder was accurately weighed and placed in a Teflon bomb; (3) 1 ml HNO_3 and 1 ml HF were slowly added into the Teflon bomb; (4) The Teflon bomb was put in a stainless steel pressure jacket and heated to 190□ in an oven for >24 hours; (5) After cooling, the Teflon bomb was opened and placed on a hotplate at 140□ and evaporated to incipient dryness, and then 1 ml HNO_3 was added and evaporated to dryness again; (6) 1 ml of HNO_3, 1 ml of Milli-Q water and 1 ml internal standard solution of 1ppm In were added, and the Teflon bomb was resealed and placed in the oven at 190□ for >12 hours; (7) The final solution was transferred to a polyethylene bottle and diluted to 100 g by the addition of 2% HNO_3. V/Cr ratios of bulk sample (Table DR. 2) were employed to investigate the redox condition of the studied interval (Fig. 2).

2.3 Measurement of trace element concentrations in leachates

Sample preparation for measurement of trace element concentrations were largely similar to the method described above for the Zn-isotope analysis, with a few differences: 1) exclusion of treatment of the Milli-Q water and 1 N ammonium acetate to remove the exchangeable fraction; 2) The leached supernatants were dried at 80 □ and added with 0.5 ml of HNO3; 3) 5 ml Mill-Q water and 0.3 ml of 6% HNO_3 were added into the beaker at 80 □ for 2 hours to dissolve the sample. The final solution was transferred to a polyethylene bottle and diluted to 100 g by the addition of 2% HNO_3. Element abundances were analyzed on an Agilent 7700e ICP-MS at the Wuhan SampleSolution Analytical Technology Co., Ltd., Wuhan, China. The Zn concentration in carbonates is calculated from Zn contents in the

leaching solutions divided by the contents of carbonates (Zn/Ca, μg/g), the latter of which are calculated based on major elements in the bulk rocks.

Because Sr/Ca and $\delta^{18}O$ values may be altered significantly in cases of major change in carbonate precipitation rate (Lorens, 1981; Watkins et al., 2014), or during extensive carbonate diagenesis (Swart, 2015), the fact that there is insignificant co-variation between $\delta^{66}Zn$ values and these two proxies (Figs. DR2 and DR3) indicates that neither process is responsible for the observed excursion in $\delta^{66}Zn$.

3. Figures

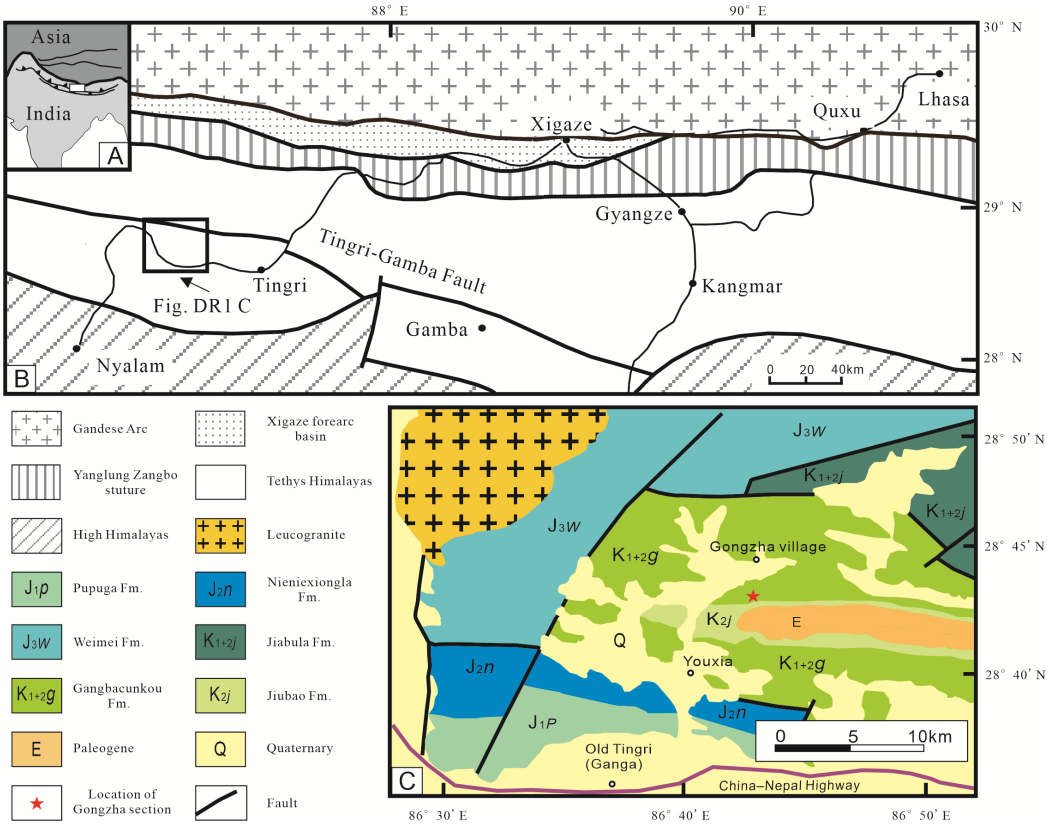

Fig. DR 1 Tectonic units of the southern Tibet (A and B) (Li et al., 2006) and geological map of the studied area showing the location of studied section (C) (modified from Hu et al., 2010).

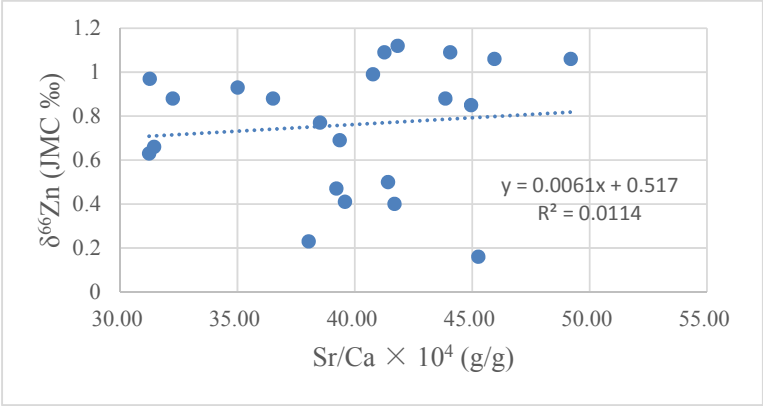

Fig. DR 2 Cross plot of δ^{66}Zn–Sr/Ca of carbonates showing the absence of co-variation. The lack of δ^{66}Zn–δ^{18}O (Fig. DR 2) and δ^{66}Zn–Sr/Ca covariance indicates that the Zn isotope shift is not related to precipitation rate or diagenesis.

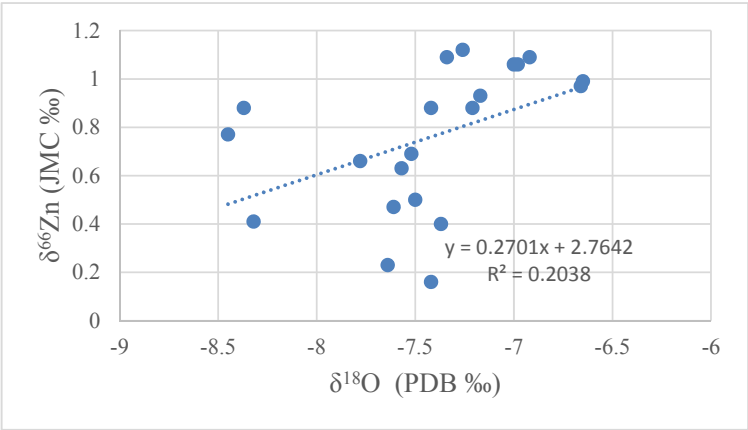

Fig. DR 3 Cross plot of δ^{66}Zn–δ^{18}O of carbonates showing the absence of co-variation. The lack of δ^{66}Zn–δ^{18}O and δ^{66}Zn–Sr/Ca (Fig. 3 in main text) covariance indicates that the Zn isotope shift is not related to precipitation rate or diagenesis.

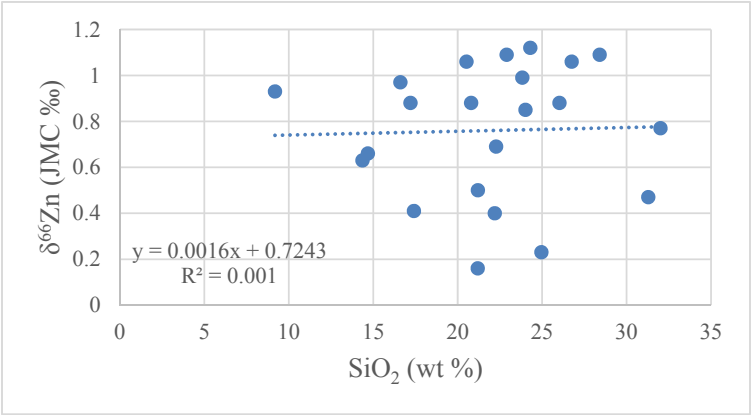

Fig. DR 4 Cross plot of δ^{66}Zn vs. SiO_2 of bulk sediments from the Gongzha section. The absence of correlation suggests that the temporal δ^{66}Zn variations are not caused by adsorption of Zn onto silicate or clay phases.

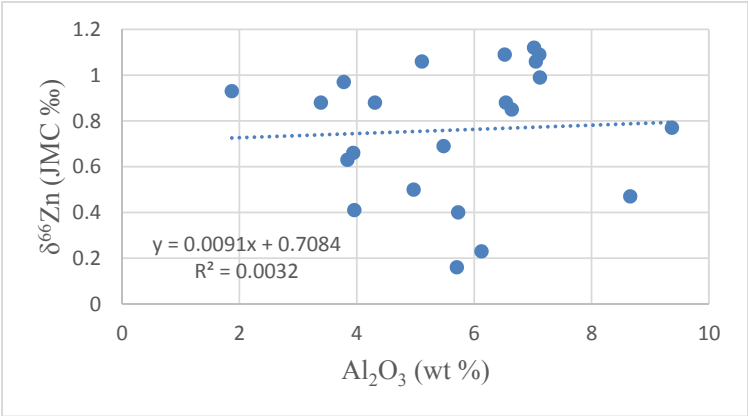

Fig. DR 5 Cross plot of δ^{66}Zn vs. Al_2O_3 of bulk sediments from the Gongzha section. The absence of correlation suggests that the temporal δ^{66}Zn variations are not caused by adsorption of Zn onto silicate or clay phases.

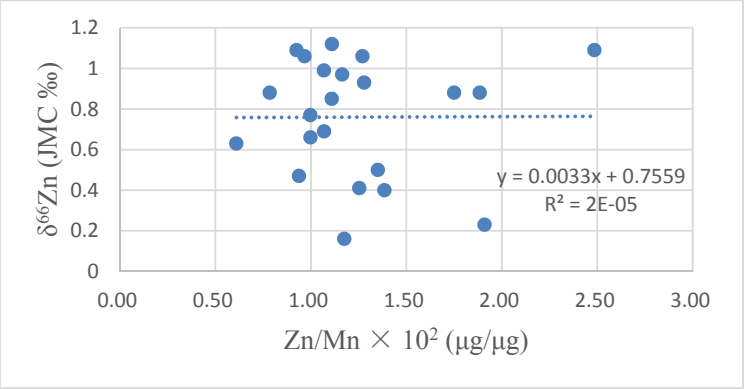

Fig. DR 6 Cross plot of δ^{66}Zn vs. Zn/Mn in leachates from the Gongzha section. The absence of correlation suggests that the temporal δ^{66}Zn variations are not caused by leaching of ferromanganese coatings.

4. Tables

Table DR 1 Weight concentration of elemental oxides (wt %)

Sample Number	Height/m	SiO_2	TiO_2	Al_2O_3	TFe_2O_3	MnO	MgO	CaO	K_2O	Na_2O	P_2O_5	LOI	Total
09GZ240	27.19	20.52	0.6	5.11	3.67	0.09	1.04	37.26	0.7	0.27	0.09	30.49	99.84
09GZ261	29.21	28.41	0.93	7.11	5.36	0.09	1.23	29.08	1.29	0.3	0.07	25.39	99.26
09GZ274	30.56	26.03	0.83	6.54	5.23	0.1	1.24	30.98	1.21	0.21	0.08	26.62	99.07
09GZ292	32.21	24.3	0.81	7.02	4.26	0.09	1.18	32.88	1.18	0.31	0.1	27.82	99.95
09GZ302	33.25	26.75	0.88	7.05	5.43	0.09	1.32	30.4	1.32	0.22	0.1	26.09	99.65
09GZ333	36.1	23.83	0.69	7.12	5.22	0.11	1.24	32.49	1.01	0.13	0.25	27.56	99.65
09GZ349	37.49	24.02	0.76	6.64	6	0.09	1.38	31.61	1.06	0.19	0.12	27.28	99.15
09GZ367	38.92	22.9	0.76	6.52	4.22	0.06	1.21	34.23	1.18	0.71	0.08	28.41	100.28
TOC1	40.05	32.01	1.08	9.37	5.99	0.04	1.22	24.66	1.92	0.37	0.11	22.62	99.39
TOC3	41	31.29	1.08	8.66	5.79	0.05	1.21	26.7	1.46	0.33	0.09	23.31	99.97
TOC6	42.05	22.28	0.67	5.48	4.85	0.06	1.11	34.94	0.74	0.22	0.6	28.39	99.34
TOC8	42.8	21.20	0.65	4.97	3.19	0.05	0.83	36.71	0.82	0.49	0.11	30.66	99.69
TOC-11	43.9	17.41	0.47	3.96	2.43	0.04	0.65	40.22	0.60	0.57	0.08	33.28	99.71
TOC-14	45.1	21.19	0.62	5.71	5.27	0.04	1.00	34.55	0.81	0.30	0.07	29.97	99.53
TOC-25	49.75	22.19	0.77	5.73	3.13	0.03	0.87	35.43	1.06	0.45	0.07	30.06	99.77
TOC-33	52.6	24.96	0.82	6.13	3.98	0.03	1.13	33.16	1.03	0.36	0.07	28.50	100.15
TOC36	53.75	17.21	0.54	3.39	2.17	0.03	0.86	41.66	0.55	0.13	0.06	33.05	99.65
TOC43	56.5	9.18	0.23	1.87	1.77	0.04	0.71	48.38	0.23	0.18	0.05	37.39	100.03
TOC54	61.8	14.36	0.36	3.84	2.68	0.04	0.95	43.27	0.34	0.14	0.09	34.16	100.23
TOC56	63.1	14.68	0.43	3.94	2.41	0.04	0.95	42.91	0.43	0.1	0.05	34.21	100.15
TOC59	64.6	20.8	0.63	4.31	2.83	0.03	0.87	39.07	0.71	0.2	0.06	31.21	100.72
09GZ654	66.14	16.61	0.4	3.78	2.74	0.06	0.97	40.96	0.43	0.1	0.06	33.21	99.32

Table DR 2 Zinc isotope ratios of leached carbonate fraction, $\delta^{18}O$ values (‰), V/Cr and Sr/Ca ratios of bulk sample, Zn concentration and Zn/Mn and Zn/Ca ratios in leachates. Sr/Ca ratio values are multiplied by 10^4. The concentration of Ca is calculated from the concentration of CaO: Ca (%) = CaO (%) × 40/56. Zn/Mn and Zn/Ca ratio values are multiplied by 10^2.

Height/m	$\delta^{66}Zn$ (‰)	2SD	$\delta^{68}Zn$ (‰)	2SD	$\delta^{68}Zn$ /$\delta^{66}Zn$	$\delta^{18}O$ (‰)	V/Cr (μg/μg)	Sr (μg/g)	Sr/Ca	Zn (μg/g)	Zn/Mn	Zn/Ca
27.19	1.06	0.04	2.13	0.01	2.00	-6.98	1.24	1309	51.63	6.50	0.97	24.42
29.21	1.09	0.01	2.16	0.01	1.99	-7.34	1.15	915	44.20	6.12	0.93	29.47
30.56	0.88	0.05	1.81	0.03	2.06	-7.21	1.23	970	44.28	5.94	0.78	26.84
32.21	1.12	0.02	2.25	0.05	2.01	-7.26	1.26	982	42.28	7.24	1.11	30.85
33.25	1.06	0.01	2.13	0.04	2.02	-7.00	1.22	998	48.59	8.69	1.27	40.03
36.10	0.99	0.00	1.99	0.02	2.01	-6.65	1.31	946	40.93	8.25	1.07	35.54
37.49	0.85	0.02	1.80	0.02	2.12	N/A	1.25	1015	48.05	6.53	1.11	28.94
38.92	1.09	0.03	2.19	0.01	2.02	-6.92	1.25	1009	43.42	10.6	2.49	43.26
40.05	0.77	0.02	1.70	0.06	2.21	-8.45	1.16	678	38.43	2.97	1.00	16.84
41.00	0.47	0.06	4.85	0.06	2.00	-7.61	1.07	748	39.21	3.21	0.94	16.82
42.05	0.69	0.06	0.92	0.06	1.97	-7.52	1.46	982	39.32	4.58	1.07	18.37
42.80	0.50	0.06	1.35	0.01	1.97	-7.50	1.31	1086	41.41	5.38	1.35	20.52
43.90	0.41	0.06	1.01	0.06	2.01	-8.32	1.54	1137	45.83	3.65	1.25	12.71
45.10	0.16	0.06	0.83	0.06	2.03	-7.42	1.35	1117	45.26	3.20	1.18	12.98
49.75	0.40	0.06	2.12	0.06	2.07	-7.37	1.10	1055	41.71	3.03	1.39	11.96
52.60	0.23	0.09	0.81	0.06	1.99	-7.64	1.11	901	38.03	4.56	1.91	19.27
53.75	0.88	0.04	0.45	0.08	1.98	-7.42	1.00	1087	39.09	4.04	1.75	13.58

56.50	0.93	0.03	1.88	0.07	2.03	-7.17	0.95	1210	36.76	3.74	1.28	10.82
61.80	0.63	0.02	1.89	0.06	3.01	-7.57	1.04	966	31.23	1.87	0.61	6.05
63.10	0.66	0.00	1.37	0.03	2.08	-7.78	1.09	964	31.51	2.72	1.00	8.87
64.60	0.88	0.05	1.78	0.01	2.03	-8.37	1.04	900	33.05	4.31	1.88	15.44
66.14	0.97	0.05	2.04	0.03	2.11	-6.66	1.10	915	31.56	4.93	1.16	16.84

References:

Bomou, B., Adatte, T., Tantawy, A.A., Mort, H., Fleitmann, D., Huang, Y., and Föllmi, K.B., 2013, The expression of the Cenomanian–Turonian oceanic anoxic event in Tibet: Palaeogeography, Palaeoclimatology, Palaeoecology, v. 369, p. 466-481.

Hu, X., Wang, C., Li, X., Fan, S., Peng, P., 2001, The Cenomanian-Turonian anoxic event in southern Tibet: A study of organic geochemistry: Chin. J. Geochem., v. 20, p. 289–295.

Hu, X., Jansa, L., Chen, L., Griffin, W. L., O'Reilly, S. Y., and Wang J., 2010, Provenance of Lower Cretaceous Wölong volcaniclastics in the Tibetan Tethyan Himalaya: Implications for the final breakup of eastern Gondwana: Sedimentary Geology, v. 223, p. 193–205.

Johnston, D.T., Macdonald, F.A., Gill, B.C., Hoffman, P.F. and Schrag, D.P., 2012, Uncovering the Neoproterozoic carbon cycle: Nature, v. 483, p. 320–324.

Junium, C.K., and Arthur, M.A., 2007, Nitrogen cycling during the Cretaceous, Cenomanian-Turonian Oceanic Anoxic Event II: Geochem. Geophys. Geosyst., 8, Q03002, doi:10.1029/2006GC001328.

Kuypers, M.M.M., van Breugel, Y., Schouten, S., Erba, E., and Sinninghe Damsté, J.S., 2004, N2-fixing cyanobacteria supplied nutrient N for Cretaceous oceanic anoxic events: Geology, v. 32, p. 853 – 856.

Li, X., Jenkyns, H.C., Wang, C., Hu, X., Chen, X., Wei, Y., Huang, Y., and Cui, J., 2006, Upper Cretaceous carbon- and oxygen-isotope stratigraphy of hemipelagic carbonate facies from southern Tibet. China: Journal of the Geological Society, London, v. 163, p. 375–382.

Li, Y., Isabel, P.M., Liu, Z., and Ma, L., 2017, Astronomical constraints on global carbon-cycle perturbation during Oceanic Anoxic Event 2 (OAE2): Earth and Planetary Science Letters, v. 462, p. 35-46.

Lorens, R.B., 1981, Sr, Cd, Mn and Co distribution coefficients in calcite as a function of calcite precipitation rate: Geochimica et Cosmochimica Acta, v. 45, p. 553–561.

Meyer, K.M., Yu, M., Lehrmann, D., van de Schootbrugge, B. and Payne, J.L., 2013, Constraints on early Triassic carbon cycle dynamics from paired organic and inorganic carbon isotope records: Earth and Planetary Sciences Letters, v. 361, p. 429–435.

Swart, P.K., 2015, The geochemistry of carbonate diagenesis: The past, present and future: Sedimentology, v. 62, p. 1233–1304.

Wan, X., Wignall, P.B., Zhao, W., 2003, The Cenomanian-Turonian extinction and oceanic anoxic event: evidence from southern Tibet: Palaeogeography Palaeoclimatology Palaeoecology, v. 199, p. 283–298.

Watkins, J.M., Hunt, J.D., Ryerson, F.J., DePaolo, D.J., 2014, The influence of temperature, pH, and growth rate on the $\delta^{18}O$ composition of inorganically precipitated calcite: Earth and Planetary Science Letters, v. 404, p. 332–343.

Zhang, X., Gao, Y., Chen, X., Hu, D., Li, M., Wang, C., Shen, Y., 2019, Nitrogen isotopic composition of sediments from the eastern Tethys during Oceanic Anoxic Event 2: Palaeogeography Palaeoclimatology Palaeoecology, v. 515, p. 123-133.